Results in Physics 7 (2017) 2118–2123

Contents lists available at ScienceDirect

Results in Physics

journal homepage: www.journals.elsevier.com/results-in-physics

Effect of copper on the growth and photochemical properties of lanthanum manganite film electrode

Guan-Ting Pan [a], Siewhui Chong [b], Thomas C.-K. Yang [a,*], Pradeep Shukla [c], Wee Siong Chiu [d], Joo Ching Juan [e]

[a] Department of Chemical Engineering and Biotechnology, National Taipei University of Technology, No. 1 Zhongxiao E. Rd. Sec. 3, Da'an District, Taipei City 106, Taiwan, ROC
[b] Department of Chemical and Environmental Engineering, University of Nottingham Malaysia Campus, Jalan Broga, 43500 Selangor, Malaysia
[c] School of Chemical Engineering, University of Queensland, Brisbane, St Lucia, QLD 4072, Australia
[d] Low Dimensional Materials Research Centre, Department of Physics, University of Malaya, 50603 Kuala Lumpur, Malaysia
[e] Nanotechnology & Catalysis Research Centre, University of Malaya, 50603 Kuala Lumpur, Malaysia

ARTICLE INFO

Article history:
Received 5 May 2017
Received in revised form 10 June 2017
Accepted 11 June 2017
Available online 16 June 2017

Keywords:
Photoelectrochemical
Photoelectrode
Photocatalysis
Hydrogen
Lanthanum
Copper

ABSTRACT

This study demonstrates that p-type copper-doped lanthanum manganite ($LaMnO_3$) film on aluminum plate substrate is a stable and efficient photo-absorber for hydrogen collection from water. Compared to using photocatalyst powder, thin-film reactor is a convenient method for industrial applications as no further filtration process is required. The copper-doped $LaMnO_3$ semiconductor films were readily deposited on aluminum plate substrates via sol-gel approach as well as spin-coating technology using photoelectrochemical cathodic current under AM 1.5 G illumination (100 mW/cm^2). The influences of copper loading on $LaMnO_3$ films in terms of surface and internal pore structure, morphology, optical and photoelectrochemical properties were comprehensively investigated. The bandgap energy and carrier density of the copper-doped $LaMnO_3$ films were found to range between 2.670–2.677 eV and 4.80×10^{15}–6.18×10^{15} cm^{-3}, respectively. The flat band potentials of these films lied in the range of −0.424 to +0.067 V vs. Ag/AgCl electrode (or −0.217 to +0.232 V vs. NHE) based on the Mott-Schottky measurements. When the molar ratio of copper in the reaction solution was higher than 0.6, the copper-doped $LaMnO_3$ film possessed the characteristics of a p-type semiconductor and yielded the best photo-performance when compared to n-type semiconductor films.

Introduction

In the past decade, doping of transition metal ions on semiconductors has been found to be an effective approach for improving the water splitting efficiency under visible-light irradiation [1–9]. However, a main issue in transition metal ions doping is the formation of metal oxide clusters, the major factor of which limits its application in water-splitting [10]. Perovskite semiconductors (ABO_3) have been demonstrated to be one of the effective photovoltaic materials for hydrogen production through water-splitting reaction due to its wide band gap of 1.5–3.0 eV [11,12]. In most previous literatures, ABO_3s are usually n-type semiconductors. Pan et al. [11] synthesized several n-type perovskite oxides (lanthanum manganite, $LaMnO_3$, lanthanum ferrate(III), $LaFeO_3$, lanthanum chromite, $LaCrO_3$, and lanthanum(III) nitrate, $LaNO_3$) using sol-gel method and achieved a photocurrent density of 0.54 mA/cm^2 in 0.1 M potassium hydroxide (KOH) solution with external bias kept at 0.5 V under illumination intensity of 100 mW/cm^2. Lervolino et al. [13] also investigated n-type $LaFeO_3$ in powder form using the solution combustion synthesis method for producing hydrogen from a PEC water-splitting reaction under UV-LED radiation. Iwashina et al. [14] prepared rhodium (Rh)-doped p-type strontium titanate photocatalyst by a solid state reaction. In recent years, novel p-type perovskite semiconductors are considered as potential material for various applications such as photoelectrochemical (PEC) water splitting, solar cells and so on [14]. Maeda et al. [15] demonstrated that Rh-doped barium titanate ($BaTiO_3$:Rh) perovskite was a stable p-type semiconductor photocatalyst for producing hydrogen from water splitting. They found that a mixture of platinum and $BaTiO_3$:Rh offered a promising performance with the amount of hydrogen evolution up to ~25 μmole for 15 h under visible light (λ > 420 nm) in an aqueous sodium iodide solution. In addition, a number of studies have

* Corresponding author.
E-mail addresses: gtpan@ntut.edu.tw (G.-T. Pan), faye.chong@nottingham.edu.my (S. Chong), ckyang@ntut.edu.tw (T.C.-K. Yang), pradeep.shukla@uq.edu.au (P. Shukla), w.s.chiu@um.edu.my (W.S. Chiu), jcjuan@um.edu.my (J.C. Juan).

http://dx.doi.org/10.1016/j.rinp.2017.06.011
2211-3797/

proven the limitations of photocatalytic powders on the recycle filtration for reuse [10,11,16]. Therefore, the development of a novel photocatalytic thin film that can produce hydrogen from photocatalytic water-splitting reaction and possess the characteristics of a p-type semiconductor properties is desirable for convenient hydrogen collection with no extra separation treatment required. Due to scarce information on p-type semiconductors, this study focuses on the synthesis and characterizations of p-type perovskite thin-film semiconductors for potential application in hydrogen production.

Results and discussion

Crystal structure analysis

Fig. 1 displays the X-ray diffraction (XRD) patterns of the copper (Cu)-doped $LaMnO_3$ ($LaMn_{1-x}Cu_xO_3$) films. As seen, the diffraction peaks of sample (a) are strong, and occur at 22.97, 32.77, 40.35, 46.91, 52.73, 58.29, 68.8, and 77.84°, indicating that sample (a) is a rhombohedral $LaMnO_3$ according to the standard cards of $LaMO_3$ (JCPDS NO. 01-075-0440). There are no other impurity diffraction peaks (Cu atoms or ternary compounds) in the XRD patterns. The diffraction peaks of the rhombohedral $LaMnO_3$ phase reduced with an increase in the molar ratio of Cu in the reaction solution, while main peak position slightly shifted to higher angle. According to Scherrer equation, the crystallite sizes of the samples are 45.44, 40.58, 37.09, 32.77, and 31.56 nm, respectively for samples (a) to (e), as listed in Table 1. The XRD results illustrated that with an increase in Cu doping, the intrinsic defects formed in $LaMnO_3$ crystal structures reduce the intensity of the $LaMnO_3$ diffraction peaks of the films and also shifted 2θ to higher angle, probably due to the induced transport and magnetic behaviors when the Mn site was occupied by Cu atoms [17].

Morphology and composition study

Fig. 2(a) displays agglomerated spherical structure on the surface of sample (a). On the other hand, Fig. 2(b) shows that in the presence of Cu, the $LaMn_{1-x}Cu_xO_3$ films demonstrate diamond-like microstructures with a highly compact surface. It was found that the morphological structure of the surface changes between samples (a) and (e), following the molar ratio of Cu in the reaction solution. Similar result was reported by Pan et al. [18], in which the micro-structure changed with the concentration of gallium (Ga) in copper indium sulfide ($CuInS_2$) film due to the replacement of In^{3+} by Ga^{3+} ions in the crystal structure. The thickness of the films estimated by FESEM was around 7.6 μm.

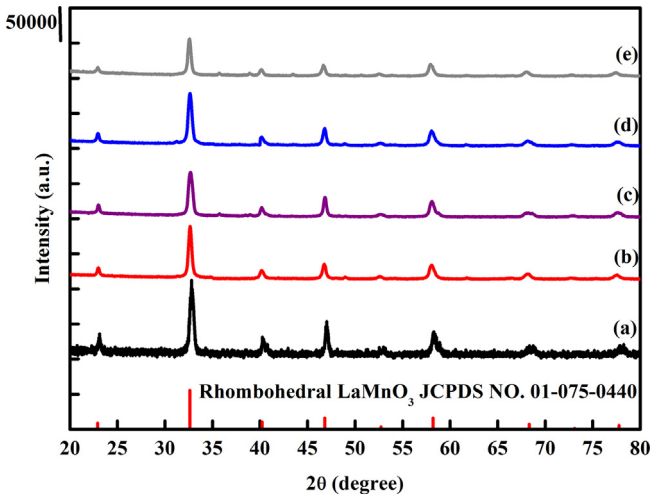

Fig. 1. XRD patterns of $LaMn_{1-x}Cu_xO_3$ films on aluminum substrates under various deposition parameters.

The surface elemental analysis results analyzed by of an energy dispersive analysis of X-ray (EDAX) for the $LaMn_{1-x}Cu_xO_3$ films are listed in Table 2. The atomic ratios of La:Mn:Cu:O for $LaMn_{1-x}Cu_xO_3$ film surfaces are in the range of 1:0.77–0.89:0.00–0.89:2.78–2.92. In accordance with the XRD results, the molar ratio of Mn in $LaMn_{1-x}Cu_xO_3$ films reduces with an increase in the molar ratio of Cu, due to Cu occupying the Mn sites in the crystal lattice. This phenomena is similar to Cheng et al. [16], who showed that sulphur (S) site was occupied by antimony (Sb) atoms in silver indium sulfide ($AgIn_5S_8$) film, leading to the change in atomic ratios and electrical structures in the samples.

Porosity and surface area characterization

Fig. 3 shows the N_2-adsorption-desorption isotherms of the $LaMn_{1-x}Cu_xO_3$ films. All samples showed type IV isotherms with H_3-hysteresis loop, indicating mesoporous structures with uniform pores. It was found that the hysteresis loop of these samples increases slowly in N_2-adsorption up to 0.9 of the relative pressure P/P_0, followed by capillary condensation with a steep increase. Hao et al. [19] reported similar hydrogen-type hysteresis loop in triangular shape and a steep desorption branch of isotherms, indicating that the narrow top pores were highly interconnected with the wider bottom pores. Fig. 4 shows the pore size distribution for all samples, with pore diameters in the range of 5–136 nm, illustrating the hierarchical porous structures. With increased Cu loading, the pore size distribution become wider along with different sizes of pore widths, with majority at around 20 nm, and 50–80 nm. It is possible that by doping Cu into the mesoporous films has changed the framework strucure of $LaMnO_3$ and increased the surface area of the materials [20]. The specific surface areas and pore structures of the samples calculated with Brunauer-Emmett-Teller (BET) theory are listed in Table 1. With an increase in the molar ratio of Cu, specific surface area, pore volume, and average pore diameter values increases in the order of: sample (e) (14.0 m^2/g, 0.089 cm^3/g, 57.0 nm) > sample (d) (12.0 m^2/g, 0.074 cm^3/g, 56.0 nm) > sample (c) (12.0 m^2/g, 0.065 cm^3/g, 52 nm) > sample (b) (11.0 m^2/g, 0.064 cm^3/g, 52.0 nm) > sample (a) (6.9 m^2/g, 0.061 cm^3/g, 50.7 nm), corresponding to the FESEM results shown in Fig. 2. These hierarchical porous structures have been proven to play an important role in enhancing the photochemical properties due to improved transport of electrons and ions [11]. Highly porous structures are able to provide plenty of space for the transport of electrolyte into the electrode material, thus effectively utilizing the electro-active materials and achieving excellent electrochemical performance [21].

PL spectra

The band gap recombinations of photoelectrons and holes of the samples are exhibited in the photoluminescence (PL) spectra in Fig. 5. The normalized PL intensities of the samples are in order of sample (e) > sample (d) > sample (c) > sample (b) > sample (a). This trend is correlated to the crystal structures, morphologies, and textural properties of the $LaMn_{1-x}Cu_xO_3$ films. As listed in Table 3, the as-prepared film samples have almost the same band gap energies (~2.670 to 2.678 eV), which agree well with some previous studies [11,22]. Bensouici et al. [23] reported that the absorption edges of the titanium dioxide (TiO_2) samples shifted towards the side with shorter wavelength when the Cu content was increased due to the incorporation of Cu^{2+} ions within the TiO_2 crystal lattice forming single TiO_2:Cu phase.

Table 1
Physical properties of $LaMn_{1-x}Cu_xO_3$ films.

Film sample	Grain size (nm)	Specific surface area (m^2/g)	Pore volume (cm^3/g)	Mean pore diameter (nm)
(a)	45.44	6.9	0.064	50.7
(b)	40.58	11	0.061	52.0
(c)	37.09	12	0.065	52.0
(d)	32.77	12	0.074	56.0
(e)	31.56	14	0.089	57.0

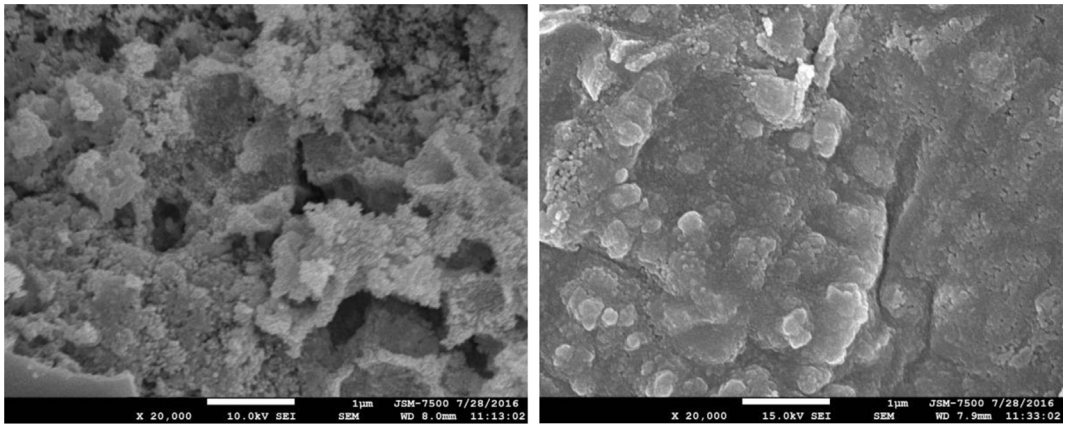

(a) (b)

Fig. 2. FESEM images showing the surface morphologies of (a) sample (a), and (b) sample (e) at 20 k(×).

Table 2
Surface elemental analysis for the $LaMn_{1-x}Cu_xO_3$ films.

Film sample	Atomic percentage from EDAX			
	La	Mn	Cu	O
(a)	1.00	0.89	0.00	2.92
(b)	1.00	0.84	0.16	2.86
(c)	1.00	0.80	0.21	2.85
(d)	1.00	0.79	0.25	2.78
(e)	1.00	0.77	0.29	2.82

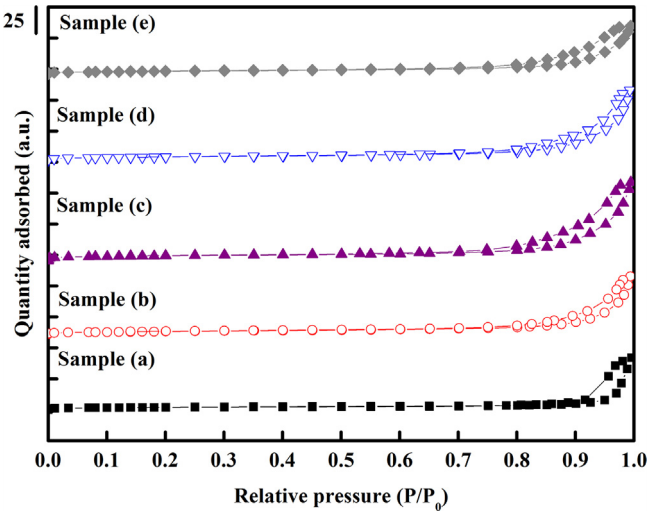

Fig. 3. N_2-adsorption-desorption isotherms of all samples.

Analysis of electrical properties

The Mott-Schottky equation was used to estimate the correlation between the semiconductor and the electrolyte in the application of solar energy and rectification [18,24,25]:

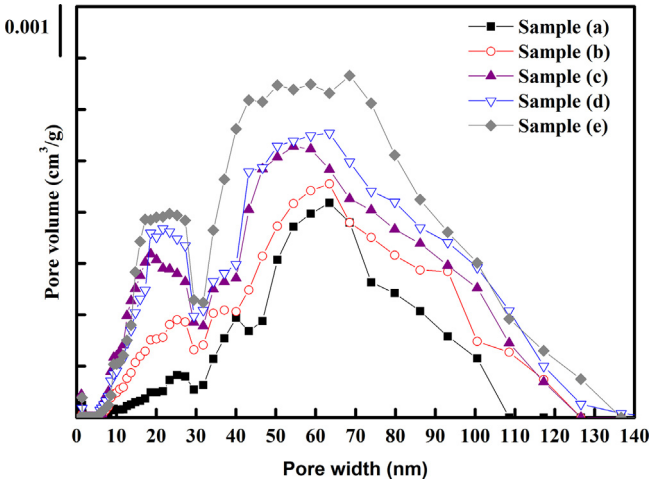

Fig. 4. Pore size distributions of all samples.

$$\frac{1}{C^2} = B\frac{2}{\varepsilon\varepsilon_0 e N_D A^2}\left(E - E_{FB} - \frac{kT}{e}\right) \quad (1)$$

where C is the space charge of layer capacitance, ε_0 is the vacuum permittivity, ε is the static dielectric constant of $LaMn_{1-x}Cu_xO_3$ semiconductor, N_D is the carrier density of the $LaMn_{1-x}Cu_xO_3$ semiconductor in the space charge region, A is the exposed surface area of the semiconductor/electrolyte barrier in the electrolyte, E is the applied potential with respect to reference electrode, e is the electric charge, E_{FB} is the flat-band potential of the $LaMn_{1-x}Cu_xO_3$ sample, which is close to the potential of Fermi level of the semiconductor, and B is equal to 1 and −1 for n- and p-type semiconductors respectively.

Using the relationship:

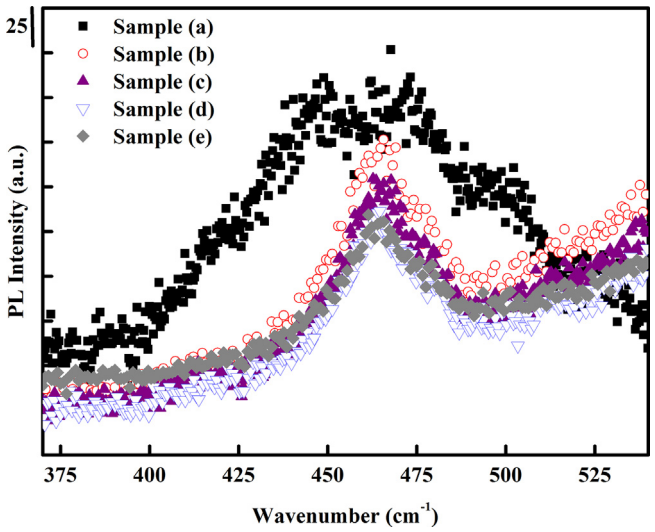

Fig. 5. PL spectra of all samples.

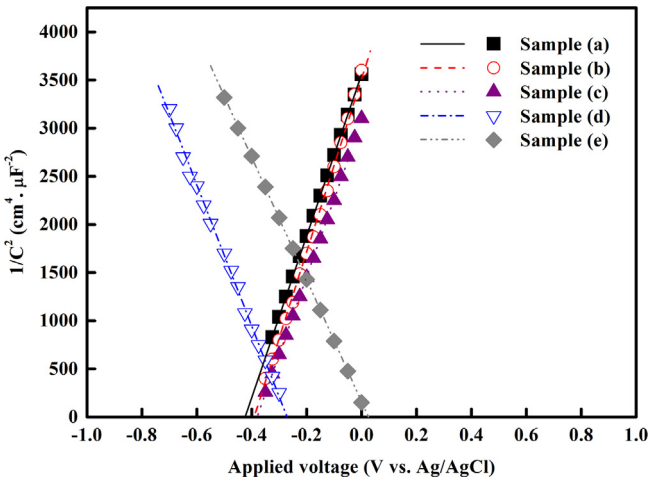

Fig. 6. Mott–Schottky plots for all samples in aqueous 0.1 M KOH solution.

$$E_0 = E_{FB} + \frac{kT}{e}, \tag{2}$$

and by plotting C^{-2} on the E-axis versus applied potential (E), E_{FB} can be determined from E_0 and the result is shown in Fig. 6. These data signal the positions of the conduction and valance bands of the $LaMn_{1-x}Cu_xO_3$ semiconductors. The dielectric constant of $LaMnO_3$ was 3.5 [26] and the area of interface was kept at 1 cm^2 in this study. The flat band potentials of these samples were found to lie in the range of −0.424 V to 0.067 V vs. Ag/AgCl electrode (or −0.217 to +0.232 V vs. NHE), as illustrated in Table 3. As can be seen, the flat band potentials (E_{FB}) of these films become more positive when the molar ratio of Cu increases. The carrier densities of samples (a)–(e) were respectively 4.80×10^{15}, 5.04×10^{15}, 5.22×10^{15}, 5.67×10^{15}, and 6.18×10^{15} cm^{-3}. The difference in the positions of the conduction and valence bands could be due to the flat band potentials and some physical properties, for instance, the carrier effective mass, the acceptor/donor, and the impurity concentration of the semiconductor [10].

Photocurrent density measurement

Fig. 7 shows the photo-performances of all samples with applied potential vs. Pt electrode in 0.1 M KOH aqueous solution under AM 1.5 G illumination (100 mW/cm^2). The photocurrent density of sample (a) was increased from 0.27 to 0.33 mA/cm^2 (sample (c)) at the external potential +0.5 V vs. Pt electrode. Similarly, the photocurrent of sample (d) was increased from −0.36 to −0.41 mA/cm^2 (sample (f)) at the external potential −0.5 V vs. Pt electrode due to the reduction of the barrier height of the Schottky layer when Cu atoms occupied the Mn site in the $LaMnO_3$ crystal lattice. Similar results were also reported by Pan et al. [25] in which better photo-performances were achieved by the cadmium sulfide (CdS) films with higher tellurium (Te) molar ratio in the reaction solution, due to the reduction of the contact resistance resulted. The better photoelectrode efficiency of sample (e) was due to the higher carrier density which enhances the photochemical reaction when the number of free electrons increase.

Materials and methods

Materials

Lanthanum nitrate hexahydrate ($La(NO_3)_3 \cdot 6\,H_2O$, 99%), citric acid ($C_6H_8O_7$, 99%), manganese(II) nitrate tetrahydrate ($Mn(NO_3)_2 \cdot 4\,H_2O$, 99%), and cupric nitrate ($Cu(NO_3)_2$, 99%) were respectively used as the sources of La^{3+}, Mn^{2+}, and Cu^{2+} ions. All chemicals were obtained from Merck without further purification. The aluminum plate substrates were cleaned with acetone, deionized water, and ethanol in an ultrasonic bath for 90 min.

The preparation method

The Cu-doped $LaMnO_3$ ($LaMn_{1-x}Cu_xO_3$) thin films were prepared via a sol-gel method developed from a reported procedure [11]. The detailed preparation parameters used in this study are shown in Table 4. The $LaMn_{1-x}Cu_xO_3$ thin films were prepared by adding 5 M $La(NO_3)_3$, various amounts of 5 M $Mn(NO_3)_2$ and $Cu(NO_3)_2$ in 1 M $C_6H_8O_7$, followed by 24-h stirring. The obtained gel suspensions were spin-coated on commercial aluminum (Al) at 3000 rpm. The thin films were dried overnight in oven at 70 °C. After drying, the samples were heated in a furnace under argon gas at 650 °C for 4 h with a ramping rate of 5 °C/min and cooled down to room-temperature gradually.

Physical characterizations

Various characterization tests were carried out to investigate the physical properties of the $LaMn_{1-x}Cu_xO_3$ thin films. The crys-

Table 3
The electrical properties of all samples.

Sample	Carrier density (cm^{-3})	E_g (eV)	E_{FB}^{NHE} (V)	E_{CB}^{NHE} (V)	E_{VB}^{NHE} (V)	E_{FB}^{Vacuum} (V)	E_{CB}^{Vacuum} (V)	E_{VB}^{Vacuum} (V)	Type
(a)	4.80×10^{15}	2.670	−0.217	−0.386	2.284	−4.283	−4.114	−6.784	n
(b)	5.04×10^{15}	2.670	−0.184	−0.351	2.319	−4.316	−4.149	−6.819	n
(c)	5.22×10^{15}	2.675	−0.176	−0.343	2.333	−4.324	−4.158	−6.833	n
(d)	5.67×10^{15}	2.677	−0.059	−2.572	0.105	−4.441	−1.928	−4.605	p
(e)	6.18×10^{15}	2.677	+0.232	−2.283	0.394	−4.732	−2.217	−4.894	p

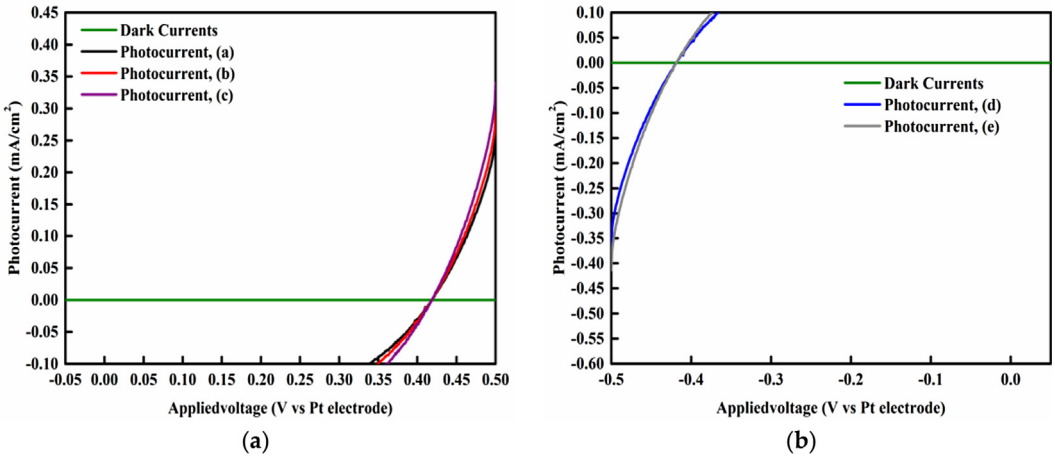

Fig. 7. The plots of photocurrent densities versus applied voltage at 0.1 M KOH electrolytes. (a) n-type $LaMn_{1-x}Cu_xO_3$ films, (b) p-type $LaMn_{1-x}Cu_xO_3$ films.

Table 4
The parameters of the sol-gel method and the molar ratios of all elements for $LaMn_{1-x}Cu_xO_3$ coated on Al plates.

Film sample/Reagent	5 M $La(NO_3)_3$/mL	5 M $Mn(NO_3)_2$/mL	5 M $Cu(NO_3)_2$/mL	1 M $C_6H_8O_7$/mL	Molar ratios of La:Mn:Cu in the films
(a)	5	5	–	10	1.0:1.0:0.0
(b)	5	4	1	10	1.0:0.8:0.2
(c)	5	3	2	10	1.0:0.6:0.4
(d)	5	2	3	10	1.0:0.4:0.6
(e)	5	1	4	10	1.0:0.2:0.8

tallinity of these films were determined by PANalytical X'Pert PRO XRD, using CuKα source radiation (λ = 1.5405 Å), with accelerating voltage 40 kV, current of 30 mA, and scan range at 2θ from 20 to 80°. The microstructures of the samples were carried out by JEOL, JSAM 6700F FESEM, and analysis of film chemical compositions was investigated with EDAX. The accelerating voltage of FESEM and Magnification of EDAX were set at 15 kV and 200(×), respectively. The band gap energy and the recombination of photoelectrons and holes were obtained using Dongwoo Optron PL spectra, with an excitation light of 325 nm. The specific surface area, pore volume, and size were measured using Micromertics ASAP 2020 BET by Barrett-Joyner-Halenda (BJH) method.

Measurement of photo-response properties

The flat-band potential test was carried out in a 250 mL Pyrex electrolytic cell containing 0.1 M KOH electrolyte using a computer-controlled potentiostat (Autolab Model PGSTAT 30) equipped with frequency-response analyzer (Autolab FRA2 modules). Before every experiment, the KOH electrolyte was degassed by purging with high-purity nitrogen gas for 60 min and ultrasonicated treatment for 30 min. The $LaMn_{1-x}Cu_xO_3$ films, the platinum plate electrode (both with an average area of 1 cm^2), and the Ag/AgCl electrode were respectively the working, counter, and reference electrodes. A silver wire was attached to the conducting layer of $LaMn_{1-x}Cu_xO_3$ films with silver paste, and the contacts and edges of the films were sealed with epoxy resin. The $LaMn_{1-x}Cu_xO_3$ films were then dried overnight at room-temperature. The Mott-Schottky plots were obtained using the impendence frequency analysis with frequency of 10 kHz. With regard to photo-response properties measurement, the solar light used was 300 W Xenon short arc lamp (Perkin Elmer Model PE300UV), fixed at 100 mW/cm^2. The photochemical properties were studied with the computer-controlled potentiostat operated in the range of the applied potentials of −0.5 to +0.5 V vs. the Pt plate electrode at a scanned rate of 5 mV/s.

Conclusions

In conclusion, a readily-handled approach was successfully developed to synthesize p-type Cu-doped $LaMnO_3$ films on aluminium plate substrates with varying Cu content. The amount of Cu was found to significantly affect the crystal structure, electrical, and optical properties of the films. XRD patterns indicate that pure rhombohedral $LaMnO_3$ crystal structure is the major phase of the films with no other impurity diffraction peaks found. The diffraction peak intensity of the rhombohedral $LaMnO_3$ phase reduces with the rising Cu concentration in these films. The band gap energies, carrier densities and flat band potentials of these samples were respectively 2.670–2.677 eV, 4.80×10^{15}–6.18×10^{15} cm^{-3}, and −0.217 – +0.232 V vs. NHE. The maximum photocurrent density was found to be −0.41 mA/cm^2 (with an external potential set at −0.5 V vs. Pt electrode) under 100 mW/cm^2 AM 1.5 irradiation. These results show that p-type Cu-doped $LaMnO_3$ film on aluminium plate substrates is a promising potential photo-absorber for solar hydrogen production applications.

Author contributions

Guan-Ting Pan wrote the paper and conducted the experiments. Thomas C.-K. Yang and Pradeep Shukla conceived and designed the experiments; Wee Siong Chiu and Siewhui Chong analyzed the data; and Joo Ching Juan contributed reagents/materials/analysis tools.

Acknowledgments

The partial financial supports from the Ministry of Science and Technology of the Republic of China, ROC (MOST – R.O.C. 104-2119-M-027-001) and Presidents' Forum of Southeast Asia and Taiwan Universities, SATU Grant (RU018B-2016 and RU018M-2016) are gratefully appreciated.

References

[1] Yang X-J, Shu W, Sun H-M, Wang X-B, Lian J-s. Preparation and photocatalytic performance of Cu-doped TiO_2 nanoparticles. T Nonferr Metal Soc 2015;25:504–9.

[2] Suttiponparnit K, Tiwari V, Sahu M, Biswas P, Suvachittanont S, Charinpanitkul T. Effect of Pt or Pd doping on stability of TIO_2 nanoparticle suspension in water. J Ind Eng Chem 2013;19:150–6.

[3] Bzdon S, Góralski J, Maniukiewicz W, Perkowski J, Rogowski J, Szadkowska-Nicze M. Radiation-induced synthesis of Fe-doped TiO_2: characterization and catalytic properties. Radiat Phys Chem 2012;81:322–30.

[4] Xu F, Mei J, Zheng M, Bai D, Wu D, Gao Z, Jiang K. Au nanoparticles modified branched TiO_2 nanorod array arranged with ultrathin nanorods for enhanced photoelectrochemical water splitting. J Alloy Compd 2017;693:1124–32.

[5] Rodríguez MH, Melián EP, Santiago DG, Díaz OG, Navío J, Rodríguez JD. No photooxidation with TiO_2 photocatalysts modified with gold and platinum. Appl Catal B 2017;205:148–57.

[6] Xu F, Bai D, Mei J, Wu D, Gao Z, Jiang K, et al. Enhanced photoelectrochemical performance with in situ Au modified TiO_2 nanorod arrays as photoanode. J Alloy Compd 2016;688:914–20.

[7] Grabowska E, Marchelek M, Klimczuk T, Trykowski G, Zaleska-Medynska A. Noble metal modified TiO_2 microspheres: surface properties and photocatalytic activity under UV–vis and visible light. J Mol Catal A Chem 2016;423:191–206.

[8] Yan Y, Lee J, Cui X. Enhanced photoelectrochemical properties of Ta-TiO_2 nanotube arrays prepared by magnetron sputtering. Vacuum 2017;138:30–8.

[9] Solís-Casados D, Escobar-Alarcón L, Gómez-Oliván L, Haro-Poniatowski E, Klimova T. Photodegradation of pharmaceutical drugs using Sn-modified TiO_2 powders under visible light irradiation. Fuel 2017.

[10] Cheng K-W, Huang C-M, Pan G-T, Chang W-S, Lee T-C, Yang TC. The physical properties and photoresponse of $AgIn_5S_8$ polycrystalline film electrodes fabricated by chemical bath deposition. J Photochem Photobiol, A 2007;190:77–87.

[11] Pan G-T, Chong S, Pan K-L, Chang M-B, Yang TC-K, Shukla P. The study of photoelectrochemical properties of $LaMnO_3$, $LaFeO_3$, $LaCrO_3$, and $LaNiO_3$ photoelectrodes for hydrogen production. Clean Technol Environ Policy 2017:1–9.

[12] Surendar M, Sagar T, Raveendra G, Kumar MA, Lingaiah N, Rao KR, et al. Pt doped $LaCoO_3$ perovskite: a precursor for a highly efficient catalyst for hydrogen production from glycerol. Int J Hydrogen Energy 2016;41:2285–97.

[13] Iervolino G, Vaiano V, Sannino D, Rizzo L, Ciambelli P. Production of hydrogen from glucose by $LaFeO_3$ based photocatalytic process during water treatment. Int J Hydrogen Energy 2016;41:959–66.

[14] Iwashina K, Kudo A. Rh-doped $SrTiO_3$ photocatalyst electrode showing cathodic photocurrent for water splitting under visible-light irradiation. J Am Chem Soc 2011;133:13272–5.

[15] Maeda K. Rhodium-doped barium titanate perovskite as a stable p-type semiconductor photocatalyst for hydrogen evolution under visible light. ACS Appl Mater Interfaces 2014;6:2167–73.

[16] Cheng K-W, Huang C-M, Pan G-T, Chang W-S, Lee T-C, Yang TC. Preparation and photoelectrochemical applications of chemically synthesized Sb-doped p-$AgIn_5S_8$ film electrodes. Phys B 2009;404:1264–70.

[17] Yang S, Li T, Gu B, Du Y, Sung H, Hung S, et al. Ferromagnetism in Mn-doped CuO. Appl Phys Lett 2003;83:3746–8.

[18] Pan G-T, Lai M-H, Juang R-C, Chung T-W, Yang TC-K. The preparation and characterization of Ga-doped $CuInS_2$ films with chemical bath deposition. Sol Energy Mater Sol Cells 2010;94:1790–6.

[19] Kruk M, Jaroniec M. Gas adsorption characterization of ordered organic-inorganic nanocomposite materials. Chem Mater 2001;13:3169–83.

[20] Gédéon A, Massiani P, Babonneau F. Zeolites and related materials: trends targets and challenges (set). In: 4th International Feza Conference, 2–6 September 2008, Paris, France. Vol. 174. Elsevier; 2008.

[21] Tsai Y-C, Yang W-D, Lee K-C, Huang C-M. An effective electrodeposition mode for porous MnO_2/Ni foam composite for asymmetric supercapacitors. Materials 2016;9:246.

[22] Huang H, Sun G, Hu J, Jiao T. Single-step synthesis of $LaMnO_3$/MWCNT nanocomposites and their photocatalytic activities. Nanomater Nanotechnol 2014;4:4–27.

[23] Bensouici F, Bououdina M, Dakhel A, Tala-Ighil R, Tounane M, Iratni A, et al. Optical, structural and photocatalysis properties of Cu-doped TiO_2 thin films. Appl Surf Sci 2016.

[24] Garskaite E, Pan G-T, Yang TC-K, Huang S-T, Kareiva A. The study of preparation and photoelectrical properties of chemical bath deposited Zn, Sb and Ni-doped $CuInS_2$ films for hydrogen production. Sol Energy 2012;86:2584–91.

[25] Pan G-T, Shen TF-R, Lai M-H, Juang R-C, Yang TC-K. The preparation and characterization of $CdS_{1-x}Te_x$ semiconductor films for hydrogen production by the chemical bath deposition method. Sol Energy Mater Sol Cells 2011;95:2524–30.

[26] Laiho R, Lisunov K, Lähderanta E, Stamov V, Zakhvalinskii V, Colomban P, et al. Lattice distortions, magnetoresistance and hopping conductivity in $LaMnO_{3+\delta}$. J Phys: Condens Matter 2004;17:105.